Pyridine Nucleotide Complexes with *Bacillus anthracis* Coenzyme A-Disulfide Reductase: A Structural Analysis of Dual NAD(P)H Specificity[†,‡]

Jamie R. Wallen,[§] Carleitta Paige,[§] T. Conn Mallett,[§,⊥] P. Andrew Karplus,[∥] and Al Claiborne*[,§]

Center for Structural Biology, Wake Forest University School of Medicine, Winston-Salem, North Carolina 27157, and Department of Biochemistry and Biophysics, Oregon State University, Corvallis, Oregon 97331

Received February 6, 2008; Revised Manuscript Received March 10, 2008

ABSTRACT: We have recently reported that CoASH is the major low-molecular weight thiol in *Bacillus anthracis* [Nicely, N. I., Parsonage, D., Paige, C., Newton, G. L., Fahey, R. C., Leonardi, R., Jackowski, S., Mallett, T. C., and Claiborne, A. (2007) *Biochemistry 46*, 3234−3245], and we have now characterized the kinetic and redox properties of the *B. anthracis* coenzyme A-disulfide reductase (CoADR, BACoADR) and determined the crystal structure at 2.30 Å resolution. While the *Staphylococcus aureus* and *Borrelia burgdorferi* CoADRs exhibit strong preferences for NADPH and NADH, respectively, *B. anthracis* CoADR can use either pyridine nucleotide equally well. Sequence elements within the respective NAD(P)H-binding motifs correctly reflect the preferences for *S. aureus* and *Bo. burgdorferi* CoADRs, but leave questions as to how BACoADR can interact with both pyridine nucleotides. The structures of the NADH and NADPH complexes at ca. 2.3 Å resolution reveal that a loop consisting of residues Glu180-Thr187 becomes ordered and changes conformation on NAD(P)H binding. NADH and NADPH interact with nearly identical conformations of this loop; the latter interaction, however, involves a novel binding mode in which the 2′-phosphate of NADPH points out toward solvent. In addition, the NAD(P)H-reduced BACoADR structures provide the first view of the reduced form (Cys42-SH/CoASH) of the Cys42-SSCoA redox center. The Cys42-SH side chain adopts a new conformation in which the conserved Tyr367′-OH and Tyr425′-OH interact with the nascent thiol(ate) on the flavin *si*-face. Kinetic data with Y367F, Y425F, and Y367,425F BACoADR mutants indicate that Tyr425′ is the primary proton donor in catalysis, with Tyr367′ functioning as a cryptic alternate donor in the absence of Tyr425′.

In *Bacillus subtilis*, diamide-mediated disulfide stress affects the transcription of more than 20% of all genes (*1*); the inductions observed for the genes encoding thioredoxin, thioredoxin reductase, cysteine synthetase A, and other putative Cys biosynthesis genes have been taken to suggest that free Cys may play a role in *B. subtilis* analogous to that played by GSH in other organisms. Indeed, *B. subtilis* lacks GSH, and Cys is the major low-molecular weight thiol (*2*). Very recently, Hochgräfe et al. (*3*) demonstrated a 6-fold increase in protein-associated ^{35}S radioactivity in *B. subtilis* cells stressed with diamide in the presence of [^{35}S]Cys (and chloramphenicol, inhibiting protein synthesis); over 80% of the ^{35}S label incorporated into proteins could be removed by treatment with disulfide reductants. These results have been taken to support the conclusion that *S*-thiolation by Cys represents a general, reversible mechanism for protection and regulation of protein-SH groups during disulfide (and other oxidative) stresses in *B. subtilis*. A complementary report (*4*) showed that the redox-regulated *B. subtilis* OhrR protein was *S*-thiolated on Cys15 in cells challenged with cumene hydroperoxide; in addition to Cys, mixed disulfides were also identified with CoASH and with a new 398-Da thiol of as-yet-unknown structure. In contrast, in other *Bacillus* species, CoASH rather than Cys is the major low-molecular weight thiol, with ∼45% of the total CoASH in *Bacillus megaterium* spores being present as soluble protein-SSCoA (*5*). Also, mature *B. megaterium* spores were shown (*6*) to contain a flavoprotein disulfide reductase that catalyzed the NADH-dependent reduction of CoA-disulfide (CoAD)[1] → 2CoASH; the 75% reduction of protein-SSCoA (to protein-SH plus CoASH) observed during spore germination (*5*) was linked to this enzyme.

[†] This work was supported by National Institutes of Health (NIH) Grant GM-35394 (to A.C.), by a grant from the Southeast Regional Center of Excellence for Biodefense and Emerging Infections (SERCEB; to A.C.), and by National Science Foundation grant MCB-9982727 (to P.A.K.). C.P. was the recipient of a Graduate Fellowship from the U.S. Department of Homeland Security (DHS). SERCEB is supported by an award from the NIH (National Institute of Allergy and Infectious Diseases; NIAID). The DHS Scholarship and Fellowship Program is administered by the Oak Ridge Institute for Science and Education (ORISE) through an interagency agreement with the U.S. Department of Energy (DOE). ORISE is managed by Oak Ridge Associated Universities under DOE contract number DE-AC05-06OR23100. The findings, opinions, and recommendations expressed in this paper are those of the authors and are not necessarily those of NIAID, SERCEB, NIH, DHS, DOE, or ORISE. Data for this study were measured at beamline X26C of the National Synchrotron Light Source. Financial support comes principally from the Offices of Biological and Environmental Research and of Basic Energy Sciences of the DOE, and from the National Center for Research Resources of the NIH.

[‡] Coordinates have been deposited with the Protein Data Bank under the file names 3CGB, 3CGC, 3CGD, and 3CGE.

* To whom correspondence should be addressed. Tel: (336) 716-3914. Fax: (336) 777-3242. E-mail: alc@csb.wfu.edu.

[§] Wake Forest University School of Medicine.

[∥] Oregon State University.

[⊥] Present address: Rigaku, Sevenoaks, Kent, TN15 6QY, England.

10.1021/bi8002204 CCC: $40.75 © 2008 American Chemical Society
Published on Web 04/10/2008

Very recently, Ojha et al. (*7*) have classified coenzyme A-disulfide reductase (CoADR) as one of the prototype enzymes of the NADH Peroxidase/Oxidase and CoAD Reductase (POR) subgroup [also previously identified as Group 3 of the PNDOR family (*8*)] of the two dinucleotide binding domains flavoproteins superfamily. A critical distinction between CoADR and all other PNDOR enzymes, including the Group 1 and Group 2 enzymes (*7*), lies in the fact that CoADR is the only disulfide reductase that uses a single active-site Cys in catalysis (*9*−*11*). The recent crystal structure for *Staphylococcus aureus* CoADR [SACoADR (*12*)] revealed the resting state of the enzyme as containing a mixed disulfide of this Cys (SACoADR Cys43) with CoASH; this nonflavin redox center plays an essential role in catalysis. The structure also identified two Tyr residues in the active site, Tyr361′ and Tyr419′, that were proposed to be important in catalysis.

Furthermore, a set of sequence motifs was developed to allow identification of other members of the CoADR class. On this basis, we have now identified the NADH-dependent CoADR in *B. megaterium* (*E* value $5e^{-75}$)[2]; CoADRs have also been identified in *Bacillus anthracis* and other members of the *Bacillus cereus* group (*12*), but not in *B. subtilis* 168.[3] In *B. anthracis* Ames, we identified a second, multimodular CoADR isoform as well, in which the CoADR module is linked to a C-terminal rhodanese homology domain [RHD (*12*)]. Recent transcriptome analyses (*13*) have shown that BACoADR (BA1263) and CoADR-RHD (BA0774) are expressed in waves III and V, respectively, during growth and sporulation of *B. anthracis* Sterne. The presence of BACoADR in the fractured spore was confirmed by proteomics analysis (*14*), providing an additional link with the NADH-dependent CoADR purified from *B. megaterium* spores (*6*). BACoADR was also identified within the cytoplasmic proteome of *B. anthracis* UM23C1-2 during exponential growth in rich medium (*15*), suggesting that it plays a general role in thiol-disulfide homeostasis. Other multimodular proteins that include a CoADR module have been identified in the category A biodefense pathogen *Clostridium botulinum* [CoADR-RHD-SirA-COG2210 (*16*)] and in the antitumor agent *Clostridium novyi-NT* [CoADR-RHD (*17*)].

As in *S. aureus* (*9*), and in an interesting contrast with respect to *B. subtilis* (*2*), CoASH is the major low-molecular weight thiol in *B. anthracis* (*18*), *B. megaterium* (*6*), and *B. cereus* (*19*), as well as the human pathogen *Borrelia burgdorferi* (*20*). While the *S. aureus* CoADR expresses a preference for NADPH, the enzymes from *B. megaterium* and *Bo. burgdorferi* prefer NADH. In contrast, an analysis of the NAD(P)H-binding motif for the *B. anthracis* CoADR was suggestive of a dual specificity for the pyridine nucleotide substrate. We have undertaken kinetic and spectroscopic studies of BACoADR and selected active-site mutants and also present the crystal structures for oxidized wild-type BACoADR and for reduced enzyme complexes with the product CoASH and either NADH or NADPH. These results add to our understanding of catalysis by this PNDOR Group 3 disulfide reductase, demonstrating that BACoADR exhibits dual specificity with respect to the NAD(P)H substrate and revealing how residues that serve to discriminate between NADH and NADPH in other PNDOR enzymes serve to promote recognition of both pyridine nucleotides in BACoADR.

EXPERIMENTAL PROCEDURES

Expression and Purification of Wild-Type and Mutant BACoADRs. Genomic DNA from *B. anthracis* Ames was provided by Dr. Arthur Friedlander, U.S. Army Medical Research Institute of Infectious Diseases. *B. anthracis* CoADR (NP_843735; "pyridine nucleotide-disulfide oxidoreductase, class I") was expressed with an N-terminal His-tag provided by the pTrcHisC plasmid vector in *Escherichia coli* B834(DE3) cells. These cells were grown in an 8-L culture (10 × 800 mL in 2.8-L Fernbach flasks) of tryptone-yeast extract-phosphate medium (*21*) supplemented with 30 mM glucose and 100 μg/mL chloramphenicol at 37 °C. Cultures were induced with 1 mM isopropyl-β-D-thiogalactopyranoside at an A_{600} of 1.0 and allowed to grow 4−8 h at 37 °C. Following centrifugation at 6,220*g* for 20 min, the washed cell pellets were resuspended in a minimal volume of 25 mM sodium phosphate, pH 7.0, containing 2 mM EDTA. A small amount of DNase was added, and cells were lysed via disruption with a pneumatic cell homogenizer (Avestin EmulsiFlex-C5). After centrifuging at 39,200*g*, streptomycin sulfate was added (2% w/v) to the supernatant, with stirring, for 20 min. The supernatant obtained on subsequent centrifugation was filtered and loaded onto a Q-Sepharose HP column equilibrated in 25 mM sodium phosphate at pH 7.0. The protein was eluted with a 0 → 1 M NaCl gradient in the loading buffer; yellow fractions were pooled and loaded onto a Ni-NTA Superflow (Qiagen) column equilibrated in 50 mM sodium phosphate, pH 8.0, containing 0.5 M NaCl and 20 mM imidazole. The His-tagged BACoADR was eluted by increasing the imidazole concentration to 100 mM. The BACoADR pool was dialyzed into 50 mM potassium phosphate, pH 7.0, containing 0.5 mM EDTA, concentrated to 10 mg/mL, and flash-frozen in liquid nitrogen as 0.02−0.5-mL aliquots and stored at −80 °C. The expression and purification protocol for SeMet BACoADR was essentially identical to that described for the native protein, except that cultures were grown in MOPS medium (EZ Rich Defined Medium, Teknova), with SeMet replacing Met. Yields for the native and SeMet BACoADRs were ca. 15 mg/L of culture.

Mutant BACoADRs were generated with the QuikChange Site-Directed Mutagenesis Kit (Stratagene), using the wild-type and Y367F (for the Y367,425F double mutant) expression plasmids as templates. The presence of only the desired mutations was confirmed by sequence analysis. Protocols and yields for the BACoADR mutant proteins were very similar

[1] Abbreviations: CoAD, coenzyme A-disulfide; CoADR, coenzyme A-disulfide reductase; POR, NADH peroxidase/oxidase and coenzyme A-disulfide reductase; PNDOR, pyridine nucleotide disulfide oxidoreductase; SACoADR, *Staphylococcus aureus* coenzyme A-disulfide reductase; RHD, rhodanese homology domain; BACoADR, *Bacillus anthracis* coenzyme A-disulfide reductase; SeMet, selenomethionine; MAD,multiwavelength anomalous dispersion; NCS, noncrystallographic symmetry; EH_2, two-electron reduced enzyme; EH_4, four-electron reduced enzyme; GR, glutathione reductase; *L-san*, *Lactobacillus sanfranciscensis*; Nox, NADH oxidase; Npx, NADH peroxidase.

[2] J. Ravel, personal communication.

[3] The four lowest *E* values range from $7e^{-26}$ to $3e^{-8}$; the essential Cys43 equivalent is absent in the two closest matches, and alignments with the two more distantly related proteins are limited to the NADPH-binding domain of *S. aureus* CoADR.

Table 1: Data Collection Statistics for Native Oxidized and SeMet BACoADR and Native Complexes with NADH and NADPH

		SeMet BACoADR				
	BACoADR	edge	peak	remote	NADH	NADPH
wavelength (Å)	1.5418	0.9796	0.9791	0.9500	1.5418	1.10
space group	C2		C2			
cell dimensions						
a, b, c (Å)	169.53, 81.74, 98.37		170.26, 80.76, 98.37			
α, β, γ (°)	90, 103.97, 90		90, 103.98, 90			
resolution (Å)	2.30	2.04	1.90	2.25	2.25	2.26
reflections	380, 781	613, 414	753, 149	454, 019	226, 639	244, 820
unique reflections	58, 072	159, 053	195, 454	118, 696	59, 708	60, 599
completeness (%)	99.9 (100)[a]	98.0 (97.0)	97.5 (96.4)	98.2 (97.5)	97.2 (96.1)	99.2 (93.2)
R_{merge} (%)	9.5 (27.9)	7.7 (38.8)	8.0 (41.3)	8.2 (34.4)	8.1 (24.0)	5.8 (24.0)
I/σ	19.8 (6.0)	8.9 (3.0)	8.6 (2.9)	9.0 (3.2)	7.8 (3.5)	23.1 (5.5)

[a] Numbers in parentheses represent data for the highest resolution shell.

to that described for the native protein, except that 250 mM imidazole was used to elute the Tyr → Phe mutant proteins from the Ni Sepharose High Performance (GE Healthcare) column.

BACoADR Assays and Anaerobic Titrations. The activities of wild-type and mutant BACoADRs were measured as described earlier for SACoADR (*11*), using a Cary 50 spectrophotometer (Varian) thermostatted at 25 °C; initial rates of ΔA_{340} were corrected for NAD(P)H oxidase activities measured in parallel. Stopped-flow measurements of BACoADR activity were carried out with the Applied Photophysics DX.17 MV stopped-flow spectrophotometer (*11*), as described previously with SACoADR, except that the final BACoADR concentration on mixing was 50 nM. CoAD concentrations were varied over the range 0.5−40 μM, at fixed NAD(P)H concentrations ranging from 0.5−20 μM, and initial rates (six measurements each) were analyzed as described by Cornish-Bowden (*22*) in order to determine steady-state kinetic parameters.

Extinction coefficients for wild-type and C42S BACoADR proteins (ϵ_{453} = 11,100 M^{-1} cm^{-1} and ϵ_{440} = 13,100 M^{-1} cm^{-1}, respectively) were determined by standard methods (*11*). Anaerobic titrations followed established protocols using Agilent model 8453 and Hewlett-Packard model 8452A diode-array spectrophotometers. The anaerobic gas train used to remove residual oxygen from the nitrogen supply has been updated to include 2 Oxiclear disposable gas purifier cartridges connected in-line with copper tubing and an Oxiclear indicating oxygen trap (*23*).

Crystal Preparation and Data Collection. Thawed aliquots of the native and SeMet BACoADR proteins were buffer-exchanged into 10 mM sodium *N*-(2-hydroxyethyl)piperazine-*N*′-2-ethanesulfonic acid, pH 7.2, to give final protein concentrations of 10 mg/mL. Large, single crystals grew best in the presence of 2 mM NAD^+ or $NADP^+$, in 24-well sitting-drop plates over reservoirs of 0.5 mL 16−26% 2-methyl-2,4-pentanediol, 0.2 M magnesium acetate, and 0.1 M sodium cacodylate, pH 6.5, at 15 °C; drop sizes were 4 + 4 μL. Crystals appeared within 1 day, growing to full size in 1 week, and were flash-frozen in a nitrogen stream at 100 K after being removed from the drop. To obtain structures for the NADH and NADPH complexes, a 150 mM NAD(P)H stock solution [freshly prepared in 10 mM sodium *N*-(2-hydroxyethyl)piperazine-*N*′-2-ethanesulfonic acid, pH 7.2] was first diluted 3-fold into a suitable cryoprotectant solution (on the basis of the concentration of 2-methyl-2,4-pentanediol used with that crystal). The crystal was soaked in 10 μL of this solution for 1−5 min, during which time a color transition from yellow → faint red occurred (*24*); the crystal was then flash-frozen in a nitrogen stream at 100 K. Data sets for native BACoADR and for the BACoADR-NADH complex were collected on a Rigaku Saturn-92 CCD detector using Cu Kα radiation from a MicroMax-007 rotating anode X-ray generator; data sets for MAD and/or single-wavelength anomalous dispersion phasing with SeMet BACoADR and for the BACoADR-NADPH complex were collected at beamline X26C of the National Synchrotron Light Source, using an ADSC Quantum-4 CCD detector. The SeMet BACoADR and BACoADR-NADH data sets were indexed, integrated, and scaled in d*TREK (*25*); the native and BACoADR-NADPH data sets were processed using MOSFLM, and SCALA (*26*) and HKL2000 (*27*), respectively. Table 1 summarizes data collection statistics for native and SeMet BACoADR, and for the BACoADR-NAD(P)H complexes.

BACoADR Phasing and Structural Refinement. We initially pursued a molecular replacement strategy using the CoADR module (35% identity) from *B. anthracis* CoADR-RHD as the search model. (The structure of CoADR-RHD has been determined in this laboratory at 2.1 Å resolution with an *R*-free of 21.8% and will be the subject of a separate report.)[4] Using MOLREP (*28*) and the native BACoADR data set (to 3 Å), the CoADR portion of CoADR-RHD, with side chains changed to Ala, yielded an apparent solution for two molecules in the asymmetric unit. $2F_o - F_c$ and $F_o - F_c$ electron density maps calculated after initial rounds of rigid body refinement and simulated annealing using CNS (*29*) suffered from model bias, and attempts to refine the BACoADR model stalled at *R*-factor and *R*-free of 44 and 50%, respectively. Side chains conserved in CoADR-RHD and BACoADR were added to the poly-Ala model during this stage of refinement.

A three-wavelength MAD data set was collected with a single SeMet BACoADR crystal, but attempts to locate the 13 Se sites per monomer with SOLVE (*30*) were unsuccessful. However, an anomalous difference map calculated at 2.0 Å resolution, using the peak wavelength data set from the MAD experiment and the initial molecular replacement phases from the BACoADR model, allowed the location of 21 of the 26 expected Se sites per dimer in anomalous difference peaks (of >7σ). These sites were then used to

[4] J. R. Wallen, W. Boles, D. Parsonage, T. C. Mallett, and A. Claiborne, unpublished experiments.

Table 2: Crystallographic Refinement Statistics for Native Oxidized and SeMet BACoADR and Native Complexes with NADH and NADPH

	BACoADR	SeMet BACoADR	BACoADR-NADH	BACoADR- NADPH
resolution range (Å)	25.11−2.30	95.35−1.90	37.45−2.25	42.11−2.26
amplitude cutoff	none	none	none	none
number of amino acid residues	888[a]	888	888	888
number of waters	442	551	460	391
number of total non-hydrogen atoms	7640	7773	7735	7659
R-factor (%)	19.2	19.9	20.6	17.7
R-free (%)	23.8	23.0	24.8	21.4
stereochemical ideality				
bond length rmsd (Å)	0.008	0.012	0.009	0.007
bond angle rmsd (deg)	1.14	1.49	1.26	1.16
φ,Ψ most favored (%)	89.3	88.5	88.1	88.3
φ,Ψ additional allowed (%)	9.9	11.0	11.2	11.2
φ,Ψ generously allowed (%)	0.6	0.4	0.5	0.3

[a] BACoADR dimer.

phase the structure with SOLVE, using either the peak wavelength (single-wavelength anomalous dispersion, to 3 Å) or the complete MAD data set (to 2.5 Å). Density modification and automatic building using RESOLVE (*31, 32*) with the MAD SOLVE phases allowed 85% of the dimer to be built, and electron density maps from both the single-wavelength anomalous dispersion and MAD SOLVE/RESOLVE phases (figure of merit = 0.75) were used to build the remaining residues manually with *O* (*33*). At this point, residues Arg181-Thr187 were not visible; these were only added in the final stages of refinement. Refinement was carried out at 2.5 Å resolution using CNS with rounds of manual rebuilding, simulated annealing, energy minimization, and group *B*-factor refinement; FAD and CoAS- were added during these rounds, which led to a model with *R*-factor = 27.5% and *R*-free = 29.8%. Phase extension and density modification with SOLOMON (*34*) incorporated the 1.90 Å resolution data. During further refinement in CNS, water molecules were identified using a 3σ difference Fourier cutoff. Final rounds of refinement were performed using REFMAC5 (*35*) and COOT (*36*), resulting in *R*-factor and *R*-free values of 19.9% and 23.0%, respectively.

The final SeMet BACoADR structure was used to determine the native BACoADR by molecular replacement, and this structure was also refined in REFMAC5 with manual rebuilding in COOT. Waters (in $2F_o - F_c$ peaks greater than 1σ) were also added. Both BACoADR-NADH and BACoADR-NADPH structures were determined using oxidized BACoADR as the molecular replacement model; initial refinements using CNS were followed with TLS (*37*) plus restrained refinement in REFMAC5. Refinement statistics for all models are summarized in Table 2. NCS restraints were not used in refinement.

RESULTS AND DISCUSSION

Catalytic, Spectral, and Redox Properties of BACoADR. Protocols for the expression and purification of recombinant wild-type, C42S, and Y367F, Y425F, and Y367,425F BACoADRs differed from that used with SACoADR, in that all proteins carried an N-terminal His-tag. Earlier SACoADR assays with 100 μM NADH replacing NADPH (K_m ~0.2 μM) gave apparent k_{cat} = 4−5 s^{-1}, or ~17% that with NADPH (*11*). A more recent analysis of the *Bo. burgdorferi* CoADR (*20*) yielded apparent k_{cat} values of 14 s^{-1} and 0.3 s^{-1} with NADH and NADPH, respectively, indicating a

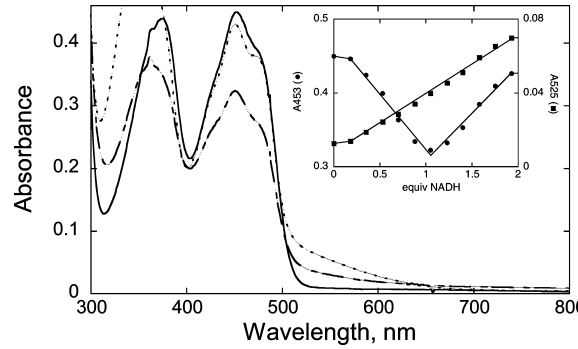

FIGURE 1: Anaerobic titration of wild-type BACoADR with NADH. The enzyme (40.8 μM, in 1.0 mL of 50 mM potassium phosphate, pH 7.0, plus 0.5 mM EDTA) was titrated with a 5.4 mM solution of NADH. Spectra shown, in order of increasing absorbance at 525 nm, correspond to the addition of 0 (-), 1.05 (-•-), and 2.1 (•••) equiv of NADH/FAD. The end point for the first phase, taken from absorbance changes at 453 and 344 nm, is 1.03 equiv of NADH/FAD; the end point for the second phase, from absorbance changes at 453 and 525 nm, is 1.97 equiv of NADH/FAD.

pyridine nucleotide preference opposite that of SACoADR.[5] Stopped-flow initial velocity measurements with BACoADR over a range of [CoAD] at several fixed [NADH] or [NADPH] yield a series of lines intersecting on the *y*-axis, consistent with a substituted-enzyme mechanism (*22*). k_{cat} with NADH = 27 s^{-1}, with K_m(NADH) = 1 μM, and K_m(CoAD) = 2 μM; with NADPH, the respective parameters are 28 s^{-1}, 3 μM, and 6 μM. The specificity constants for BACoADR with NADH and NADPH are 2.7×10^7 M^{-1} s^{-1} and 9.3×10^6 M^{-1} s^{-1}, respectively. These results demonstrate that BACoADR exhibits dual specificity with respect to the pyridine nucleotide substrate, in contrast to the CoADRs from *S. aureus* and *Bo. burgdorferi*.

Dithionite titration of BACoADR provides spectral evidence for an asymmetric EH_2 species in which one FAD per dimer is reduced; there is a 55% decrease in A_{453} on addition of 1.2 equiv of dithionite/FAD. Although there is a small increase in A_{525} at this point, there is no convincing EH_2 charge-transfer (Cys-S^- → FAD) intermediate (*8, 38, 39*), and complete flavin reduction is observed with 2 equiv of dithionite/FAD. The titration behavior observed with NADH is significantly different (Figure 1); the maximal decrease in A_{453} (only ca. 28% reduction, where 100% reduction

[5] Preparations of the NADH-dependent CoADR enzyme from *B. megaterium* were reported to be inactive with NADPH, in addition (*6*).

Scheme 1: Reductive Intermediates on NAD(P)H Titration of BACoADR[a]

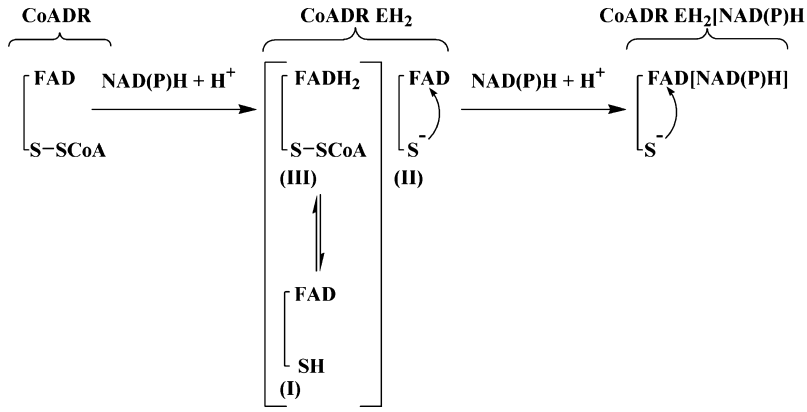

[a] Roman numeral designations for EH_2 species correspond to those used in Figure 7 of ref *40*.

represents zero absorbance at 453 nm) coincides with the addition of 1.1 equiv of NADH/FAD. Judging from the isosbestic point at 346 nm (determined from difference spectra over the titration range 0−0.7 equiv of NADH), stoichiometric oxidation of added NADH is observed at this stage. Figure 1 also indicates that a significant Cys-S^- → FAD charge-transfer component is present. As NADH is added, to 2.1 equiv/FAD, this the A_{525} component effectively doubles, commensurate with the observed *increase* in A_{453}. Essentially identical spectral changes are observed on titration with NADPH, and in both cases the dimeric EH_2 form is stabilized in the presence of up to 4 equiv of NAD(P)H/FAD (Figure 1 and Scheme 1). Since the intramolecular redox event observed as E($FADH_2$) oxidation with wild-type BACoADR requires the addition of the second equiv of NADH, it is reasonable to suggest that NADH is tightly bound to one or both subunits in the EH_2 form. Direct evidence in support of this is provided with the crystal structures described in a later section. For the BACoADR C42S mutant, dithionite titration yields complete FAD reduction, as expected (*11*), with 1 equiv/FAD. However, titrations of the mutant with either NADH or NADPH fail to yield full flavin reduction on addition of even 10−13 equiv of NAD(P)H/FAD. Absorbance changes at 340 nm and beyond 500 nm are suggestive of E[FAD-NAD(P)H] complex formation, and the limiting spectral form observed with 10.8 equiv of NADPH/FAD exhibits a largely oxidized (66% of the starting A_{440}) component.

We interpret the redox behavior of wild-type BACoADR as follows, as adapted from the model proposed by Wilkinson and Williams for *E. coli* lipoamide dehydrogenase (*40*). The dithionite titration at 1 equiv/FAD yields ca. 50% of the enzyme subunits with reduced flavin ($FADH_2$), corresponding to species IIIB (see Figure 7 of ref *40*). Since no convincing charge-transfer intermediate corresponding to species II is observed, we attribute the remaining 50% of the BACoADR subunits to species I (A or B), where the single active-site Cys42-SH of BACoADR is equivalent to the proximal Cys in lipoamide dehydrogenase. BACoADR and all PNDOR Group 3 enzymes lack the distal Cys residue that represents the interchange thiol (*8*). Given the asymmetric behavior documented for SACoADR on interaction with pyridine nucleotides (*11*), we interpret these BACoADR results in a similar asymmetric scheme, with the two-electron (dithionite) reduced BACoADR represented as E($FADH_2$, Cys42-SSCoA)/E(FAD, Cys42-SH). Complete dithionite reduction yields the EH_4 enzyme form E($FADH_2$, Cys42-SH). This behavior with dithionite, at the EH_2 state, contrasts with that reported for SACoADR, as no FAD reduction occurs with 1 equiv of dithionite in the latter case (*11*).

At 1 equiv of NADH/FAD, there is convincing evidence for ca. 50% of the total charge-transfer absorbance ultimately observed with an excess of reductant (Scheme 1); this corresponds to species II in lipoamide dehydrogenase (see Figure 7 of ref *40*). There is significant flavin reduction as well, but any E($FADH_2$-NAD^+) component is spectrally silent. Although we cannot be certain, it is likely that a significant species I component is also present. Addition of the second equiv of NADH/FAD leads to quantitative appearance of species II.

The major differences in redox behavior for SACoADR and BACoADR with NAD(P)H are (1) the presence of strong EH_2 charge-transfer absorbance in BACoADR [with 2 equiv of NAD(P)H/FAD] and (2) the effective absence of an E($FADH_2$) component in BACoADR titrated with 2 equiv of NAD(P)H/FAD. Finally, while the SACoADR C43S mutant is reduced directly with 1 equiv NADPH/FAD to give the dimeric E($FADH_2$-$NADP^+$) species (*11*), the equivalent BACoADR C42S mutant is refractory to complete reduction in titrations with either NADPH or NADH. It is of interest to note that the equivalent C44S mutant of *E. coli* lipoamide dehydrogenase was also resistant to NADH reduction in static titrations; only ca. 15% FAD reduction was observed with 1 equiv/FAD (*41*). Independent measurements of the redox potentials (FAD/$FADH_2$ couples) for the wild-type (EH_2/EH_4) and C44S mutant lipoamide dehydrogenases demonstrated that the flavin potential is 65 mV lower for the mutant (*42*).

NAD(P)H Dinucleotide-Binding Motifs. Among the four conserved sequence motifs identified by Dym and Eisenberg (*43*) as being shared by all NAD(P)H-dependent members of the GR_1 subfamily [which includes all of the PNDOR enzymes (*38, 39*)], one represents part of the $\beta\alpha\beta$ Rossmann NAD(P)H dinucleotide-binding motif. This specific motif has most recently been applied in the description and functional analysis of the two dinucleotide binding domains flavoproteins superfamily (*7*) containing both FAD- and NAD(P)H-binding motifs. Figure 2 presents a structure-based sequence alignment for the NAD(P)H-binding motifs of SACoADR (NADPH), GR [NADPH (*44*)], BACoADR (NADH/

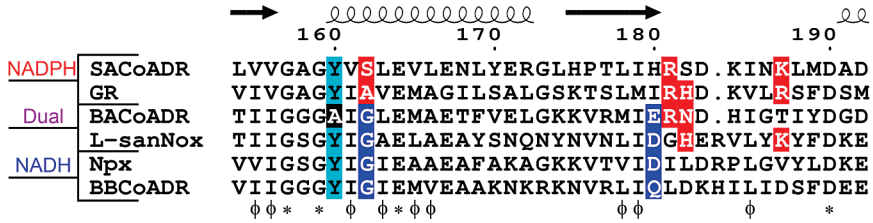

FIGURE 2: Structure-based sequence alignment for the NAD(P)H-binding motifs of selected PNDOR enzymes. Specific enzymes are identified in the text; BBCoADR represents the enzyme from *Bo. burgdorferi*. The secondary structure corresponds to SACoADR (*12*), while sequence numbering corresponds to BACoADR. Enzymes are grouped according to NAD(P)H substrate preference; red blocks represent NADPH, and blue blocks represent NADH. BACoADR and *L-san* Nox exhibit dual NAD(P)H specificity. Asterisks designate conserved residues, and positions conserving hydrophobic residues are indicated by φ.The conserved (in GR, Npx, and Nox) Tyr is highlighted in cyan.

NADPH), *L-san* Nox [NADH/NADPH (*45*)], Npx [NADH (*46*)], and the *Bo. burgdorferi* CoADR (NADH). Studies have shown that GR Ala and Arg residues at positions 162, 181, and 187 (BACoADR numbering used here for simplicity) contribute to NADPH specificity (*44, 47*) and that Npx Gly and Asp residues at positions 162 and 180 contribute to NADH specificity (*46*). The BACoADR NAD(P)H-binding motif reflects a hybrid sequence and includes both Glu180 and Arg181. In addition, the presence of Gly162 should *enable* recognition of NADH while *retaining* facile recognition of NADPH because in *E. coli* GR K_m(NADPH) actually decreased 2-fold in the corresponding Ala → Gly mutant (*47*), while K_m(NADH) decreased by 40-fold. These inferences are supported by the recently (*48*) reported structures of glutathione amide reductase, which is closely related to GR but prefers NADH (*49*), and its complex with NAD^+.

Overall Structure of Oxidized BACoADR. Although the 1.90 Å resolution of the refined SeMet BACoADR model is better than the 2.30 Å resolution for native oxidized BACoADR, the Cys42-SSCoA disulfide is partly reduced (~50%) by synchrotron radiation in the SeMet structure. We therefore discuss the native oxidized BACoADR structure, which includes residues 1−444 for both chains A and B of the biological dimer (with residues from chain B being designated by a prime symbol), two FAD cofactors, two covalently bound CoAS-, and 442 solvent waters. It has an *R*-factor of 19.2% (*R*-free = 23.8%) with reasonable geometry (Table 2). There is no electron density for the residues of the N-terminal His-tag. Although NCS restraints were not used in refinement, the two subunits of the dimer are essentially identical with a 0.2 Å C_α rmsd [DALILITE (*50*)]. As expected, BACoADR is very similar to SACoADR (PDB code 1YQZ) with a C_α rmsd = 1.7 Å for 841 atoms (COOT) in the dimer (33% identity; Figure 3). Since the SACoADR structure has already been described in detail (*12*), here we highlight the features of BACoADR that differ from those of SACoADR.

The first area of difference focuses on the covalently bound CoAS-. In the SACoADR structure (*12*), it was noted that the active-site CoAS- for chain B was less well-ordered than that for chain A and exhibited an alternate conformation for the pyrophosphate moiety. In addition, the CoAS-3′-phosphate (both chains) was observed to be entirely solvent exposed. In oxidized BACoADR, alternate conformations also exist for the CoAS-pyrophosphate in both chains, but the alternate conformations differ from those in SACoADR. More importantly, however, the CoAS-3′-phosphate in BACoADR is not fully exposed to solvent, but is anchored in the protein, connecting via hydrogen bonds with Gln18, Arg21, Arg308, and Arg441′ side chains (Figure 4); Arg21, Arg61, and Arg441′ provide for strong electrostatic interaction with the CoAS-pyrophosphate, and Arg442′ provides a cation−π stacking interaction with the adenine moiety of the bound CoAS-. Although Gln18 and Arg21 are conserved in SACoADR, they play completely different roles in CoAS-recognition in the two enzymes. As shown in Figure 4, the SACoADR Gln19 side chain provides three hydrogen bonds to the adenine and pyrophosphate components of the covalently bound CoAS-; BACoADR Gln18 instead provides a single hydrogen bond to the CoAS-3′-phosphate. While SACoADR Arg22 is engaged via both a cation−π stacking interaction with the CoAS-adenine and a single hydrogen bond with the ribose-2′-hydroxyl, BACoADR Arg21 provides three hydrogen bonds with the CoAS-pyrophosphate and 3′-phosphate.

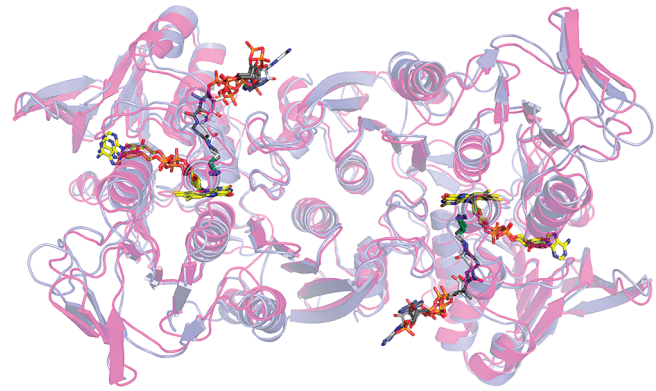

FIGURE 3: Superposition of the BACoADR dimer (slate blue) with that of SACoADR (magenta); both proteins are rendered as 50% transparent. FAD and CoAS- are color-coded by atom type, with carbon atoms colored as follows: FAD, yellow; CoAS- of BACoADR, white; CoAS- of SACoADR, gray. The view down the crystallographic 2-fold symmetry axis corresponds to a 90° forward rotation of the SACoADR dimer given in Figure 2 of ref *12*.

A second major structural difference focuses on the respective NAD(P)H-binding motifs. In oxidized BACoADR, the Glu180-Thr187 loop is poorly ordered, with weak electron density and high *B*-factors (near 45 $Å^2$ for chain A); the equivalent segment of the NADPH-binding motif in SACoADR is well-ordered and adopts a distinct conformation. This segment in fact represents the most significant main chain difference between the two structures. Disorder involving this region of the NAD(P)H-binding motif (Figure 2) has not been seen for other PNDOR enzymes (*44, 46*). Superpositions of the oxidized BACoADR structure with those of the GR(GSSG + $NADP^+$) and Npx Cys42-SO_3H-NADH complexes indicate that either a BACoADR protein conformational change must occur to allow binding of

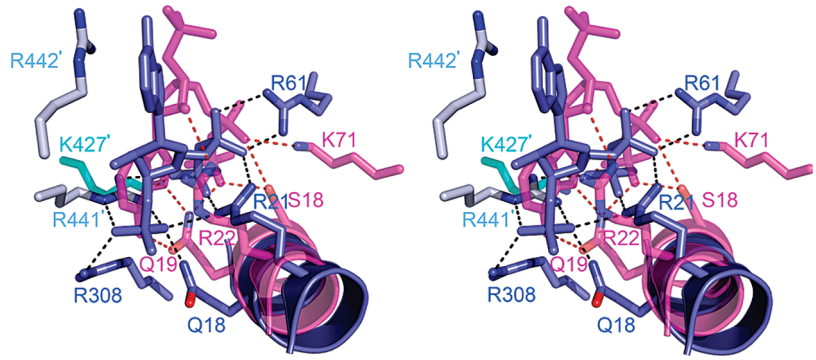

FIGURE 4: Stereoview comparing protein−CoAS- interactions in BACoADR and SACoADR. BACoADR helix α1 and the ADP-3′-phosphate moiety of CoAS- (pantetheine moiety omitted for clarity) are colored slate blue, as are carbon atoms for chain A residues; those for Arg441′ and Arg442′ (chain B) are light blue. SACoADR helix α1 and that CoAS- ADP-3′-phosphate are colored magenta, as are carbon atoms for chain A residues; those for Lys427′ (chain B) are cyan. Protein−CoAS- hydrogen-bonding interactions are given in black and red dashes for BACoADR and SACoADR, respectively. All side chains are color-coded by atom type; all elements of SACoADR are rendered as 30% transparent.

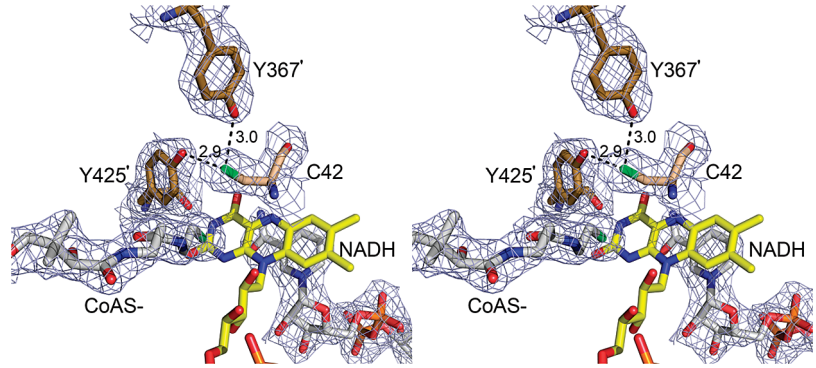

FIGURE 5: Stereoview of the BACoADR-NADH complex, focusing on the active site. The refined model is shown for the NADH-reduced Cys42-SSCoA center and includes FAD, bound NADH, and the Tyr residues from chain B. $2F_o - F_c$ density contoured at 1σ is included for all elements except FAD, and portions of the FAD, CoAS-, and NADH have been omitted for clarity. Color-coding is by atom type, as in Figure 3; carbon atoms for NADH, Cys42, and Tyr are colored gray, wheat, and sand, respectively.

NAD(P)H, or NAD(P)H must bind to BACoADR in a conformation very different from those observed in other PNDOR enzymes.

Reduced BACoADR-NADH and NADPH Complexes. Soaks of oxidized BACoADR crystals with NADH and NADPH led to reduction of the crystalline enzyme as evidenced by color changes of the crystals (see Experimental Procedures). The two models were refined at near 2.3 Å resolution to reasonable *R*-factors (Table 2). Each of the final refined models includes an NADH (Figure 5; or NADPH) in each active site and a reduced Cys42-SSCoA center, with the CoASH product remaining tightly bound and the nascent Cys42-SH side chain adopting a new conformation in which -SG interacts with Tyr367′-OH and Tyr425′-OH. The new Cys42-SG to CoASH-S distance is 4.0 Å; each CoASH is now well-ordered in the respective structure, with no alternate conformation for the CoASH-pyrophosphate as described in oxidized BACoADR. For both complexes, the two subunits of the respective dimer are essentially identical (rmsd ∼ 0.2 Å).

Comparing the BACoADR-NADH complex with oxidized BACoADR (rmsd = 0.8 Å), the largest movement occurs for the Glu180-Thr187 loop (Figure 6A), which becomes ordered and shifts up to 8 Å (maximal C_α displacement at Asp183). This change in conformation allows the formation of many new hydrogen bonds with both protein and NADH groups (Table 3). Three of the new hydrogen bonds made with NADH are from the Glu180 and Asn182 side chains to the adenine−ribose hydroxyls (Figure 6B). The conformation adopted by Glu180-Thr187 in the BACoADR-NADH complex is very similar to that found within the NADPH-binding motif of both *oxidized* SACoADR (*12*) and the Npx Cys42-SO_3H-NADH complex [with the BACoADR Glu180 side chain matching Npx Asp179, as inferred from Figure 2 (*46*)].

This simple binding mode for NADH raises the question as to how NADPH is recognized since the interactions of the Glu180 and Asn182 side chains with the 2′-hydroxyl in the BACoADR-NADH complex would be expected to discriminate against the 2′-phosphate of a canonically bound NADPH (*44, 47*). The structure of the BACoADR-NADPH complex demonstrates that binding is achieved by small shifts in the adenine−ribose pucker that allow the 2′-phosphate to point away from the enzyme surface (Figure 6B). The hydrogen bond between the Glu180-carboxylate and the adenine−ribose 3′-hydroxyl is preserved, and Asn182-ND2 retains its interaction with the bridging oxygen of the 2′-phosphate (i.e., the 2′-hydroxyl in NADH) and develops a new hydrogen bond with one of the phosphate oxygens. Arg181 also shifts its side chain conformation to allow hydrogen bonds with two of the 2′-phosphate oxygens. Finally, a new hydrogen bond is formed between Thr187-OG1 and the 3′-hydroxyl of bound NADPH. Scrutton et al. (*47*) examined the contributions of seven residues in *E. coli* GR, with respect to the preference for NADPH versus NADH. In addition to four of the human GR residues (some

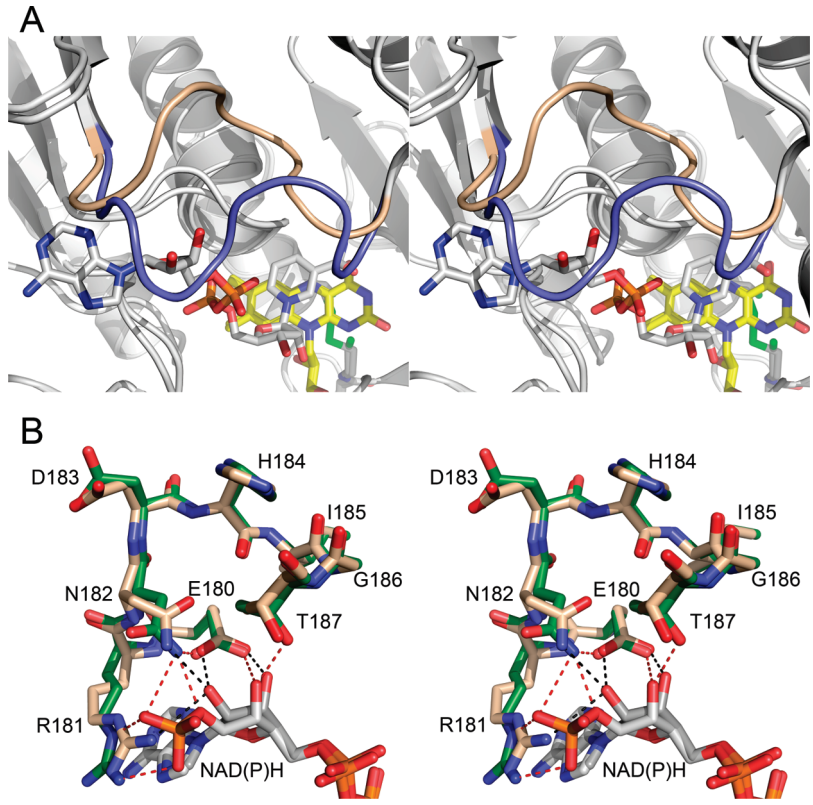

FIGURE 6: Comparison of the Glu180-Thr187 loop conformations in oxidized and NADH-reduced BACoADR. (A) Shown in stereo are the oxidized and reduced (Cys42-SH + CoASH) forms of the Cys42-SSCoA center and the two FAD centers (portions omitted for clarity), respectively, and the full bound NADH of the BACoADR-NADH complex. The Glu180-Thr187 loop conformations for oxidized and BACoADR-NADH complex forms are colored slate blue and wheat, respectively. All other protein elements are rendered in white; NADH, FAD, and Cys42-SSCoA color-coding are as in Figure 5. The superposition was performed with the respective dimers. (B) Glu180-Thr187 loop side chain conformations and NAD(P)H interactions in the BACoADR-NADH and -NADPH complexes. Color-coding is by atom type; protein carbon atoms for the complexes are colored wheat and forest green, respectively; NAD(P)H carbons are colored as in Figure 5. Hydrogen bonds involving NADH and NADPH are given in black and red dashes, respectively. As in (A), the superposition was performed with the respective dimers.

Table 3: Hydrogen-Bonding Interactions for the Glu180-Thr187 Loop in Oxidized BACoADR and in the NADH Complex

Oxidized BACoADR		BACoADR-NADH complex	
protein atoms	D···A (Å)	protein and NADH atoms	D···A (Å)
180-N···209-O	2.96	180-N···209-O	2.75
		180-O···212-N	3.24
180-OE1···198-OH	2.84	180-OE1···182-N 180-OE1···NADH-AO2*	3.35, 2.53
180-OE2···198-OH	3.03	180-OE2···158-N 180-OE2···NADH-AO3*	2.67, 2.71
		182-N···180-OG1	3.35
		182-O···210-OG1 182-O···211-N	2.73, 2.94
182-ND2···211-OD1	2.76	182-ND2···NADH-AO2*	2.82
		183-O···210-OG1	2.43
		183-OD2···211-ND2	2.79
184-O···187-OG1	2.97		
		184-NE2···189-O	2.98
186-O···343-ND2	2.88	186-O···189-N	2.88
187-O···343-ND2	3.27	187-O···345-NZ	2.65

of these are not conserved in the *E. coli* enzyme) highlighted in Figure 2 [Ala162, Arg181, His182, and Arg187 (BACoADR sequence numbering)], Ala166, Ile180, and Asp183 were included in that analysis. In addition to the analyses of BACoADR Glu180, Arg181, Asn182, and Thr187 described above, we also evaluated BACoADR Gly162, Ala166, and Asp183 for their contributions to cofactor discrimination in the BACoADR-NAD(P)H complexes. In summary, none of these residues appear to make an active contribution; the closest approach for Gly162 (Gly162-N) gives a distance of ~4.1 Å from the cofactor pyrophosphate. Ala166-C_α is ~11 Å from the nearest atom of bound NAD(P)H, and Asp183 is not conserved among GRs; it is replaced by His in the *E. coli* enzyme. In BACoADR, Asp183 is exposed to solvent as well.

Dual NAD(P)H Specificity in Lactobacillus sanfranciscensis Nox. Lountos et al. (*45*) recently reported that the Nox from *Lactobacillus sanfranciscensis* (*L-san*) oxidizes NADH and NADPH with approximately equal affinity, although an apparent 3−4-fold preference for NADH over NADPH was noted. Calculations of k_{cat}/K_m for NADH and NADPH from the data given yield values of 2.7×10^7 M^{-1} s^{-1} and 8.5×10^6 M^{-1} s^{-1}, respectively. Electron density interpreted as an active-site ADP in the *L-san* Nox crystal structure, combined

with the identification of ADP by mass spectrometry, led to the conclusion that ADP is bound to and blocks the canonical NADH-binding site. This inference led to the heterodox proposal that ADP remains bound throughout the catalytic cycle; as such, NAD(P)H access to the flavin occurs not at the expected binding site, but via an unprecedented large, *re*-face channel, which lacks the determinants of coenzyme specificity (see Figure 8 of ref *45*). This is taken further to support the conclusion that "the presence of the ADP ligand in *L.san*-Nox2 appears to be responsible. . .for the lack of substrate preference by this homologue."

Not finding this explanation attractive, our attention was drawn to the sequence of the NAD(P)H-binding motif for *L-san* Nox. The pyridine−nucleotide binding motif for *L-san* Nox (Figure 2) is entirely consistent with a subtle mechanism for dual NAD(P)H specificity similar to that described above for BACoADR. Although there is no basic residue equivalent to BACoADR Arg181, there are basic residues equivalent to Asn182 (Nox His181) and Thr187 (Nox Lys187) that could support dual coenzyme specificity for *L-san* Nox. To test the plausibility of this reinterpretation of the *L-san* Nox data, we have superimposed the BACoADR-NADPH structure with that of the *L-san* Nox-ADP complex (chain A; PDB code 2CDU). Without invoking the controversial conclusions that (1) ADP remains bound throughout the catalytic cycle and (2) NAD(P)H accesses the flavin through a promiscuous *re*-face channel, we can demonstrate that this alternate NADPH conformation positions the 2′-phosphate away from the Nox protein interior. Nox His181 is indeed structurally equivalent to BACoADR Asn182 and, with a change in the side chain rotamer, can provide a strong hydrogen bond (2.99 Å) with the bridging oxygen (O2′A) of the NADPH 2′-phosphate in this model. Nox Lys187 is structurally equivalent to BACoADR Thr187 [and to GR Arg224 in the GR(GSSG + $NADP^+$) complex (*44*)] and can also interact with the 2′-phosphate on adjustment of the side chain rotamer. While Nox Lys213 is not structurally equivalent to BACoADR-NADPH Arg181, Lys213-NZ is proximal to the Arg181 guanidinium moiety in the overlay. Its distance of ∼5 Å from the 2′-phosphate would require some change in the Nox-NADPH conformation in order to establish a favorable interaction.

We should also note that the putative bound ADP in the Nox crystal structure (*45*) may in fact be NAD^+ or a mixture of NAD^+ and ADP. A major 686-Da species observed in the mass spectrometric analysis but not discussed (see Figure S1 of ref *45*), fits the *m*/*z* calculated for the sodium (Na^+, 23 Da) adduct of NAD^+ (663 Da). In this light, half or more of the ADP modeled into the Nox structure could represent a bound NAD^+ in which only the ADP portion is ordered; such partial ordering of nicotinamide dinucleotides is very common among PNDOR enzymes, as is illustrated by the GR(GSSG + $NADP^+$) crystal structure (*44*), for which only the 2′,5′-ADP moiety of bound $NADP^+$ is included in the final refined model. In conclusion and without offering any support for the *L-san* Nox kinetic analysis, the BACoADR mechanism for NAD(P)H recognition may also provide for the dual specificity reported for *L-san* Nox. One distinct advantage in this model is that it avoids other controversial, and in our view, unnecessarily heterodox proposals for PNDOR enzyme−substrate recognition.

BACoADR Ala160-for-Tyr Replacement. Although not a specificity determinant for NAD(P)H recognition, GR Tyr197 does play an important role in NADPH binding (*44*). From the alignment given in Figure 2, this Tyr is not conserved in BACoADR but is replaced by Ala. This Tyr is conserved in Npx and in all known functional NADH oxidases [Nox; PNDOR Group 3, see above (*12, 45*)] and GRs (*51*), but not in other PNDOR enzymes; it is present in several of the CoADRs identified in bacteria (including SACoADR and the *Bo. burgdorferi* and *B. megaterium* CoADRs) and archaea (*12*) but is often replaced with Ala or other aliphatic residue. Replacement of this conserved (in GR, Npx, and Nox) Tyr residue with Ala raises an important question about the molecular spring mechanism for hydride transfer (*51*), as it relates to BACoADR. The molecular spring hypothesis was derived from the observation that the GR reductive half-reaction is seriously compromised in the Y197S mutant. The apparent k_{cat} is 14% that of wild-type GR, and the rate constant for the limiting step in reduction (conversion to the EH_2 charge-transfer intermediate) is decreased 20-fold. The k_{cat} values for SACoADR (Tyr158) and BACoADR (Ala160) with NADPH are 27 s^{-1} (*11*) and 28 s^{-1}, respectively; although the point has not been confirmed experimentally (e.g., by mutagenesis), it appears that any molecular spring function for SACoADR Tyr158 has a minimal impact on turnover.

Structure of the Reduced Cys42-SSCoA Center. As described in earlier studies with SACoADR (*9, 11, 12*), a key mechanistic contrast with GR and other PNDOR Group 1 and 2 enzymes (*8*) involves the single active-site Cys (BACoADR Cys42), which both receives electrons from the flavin during Cys42-SSCoA reduction (and serves as the charge-transfer donor to FAD in the EH_2 form; Figure 1) and engages the CoAD substrate as the nucleophile in the thiol−disulfide exchange reaction. In both the NADH and NADPH complexes with BACoADR, while the respective nicotinamides are stacked on the *re*-face of the flavin isoalloxazine, the Cys42-SSCoA centers on the flavin *si*-face are reduced. In these structures (Figures 5 and 7), the CoASH product remains well-ordered in its binding pocket, suggesting that it binds rather tightly; in solution assays, the dissociation of CoASH product may be enhanced by excess CoAD. There are no crystal contacts involved in this CoASH: protein interaction. A slight shift (∼1.7 Å) in position of the bound CoASH-S accompanies reduction, such that CoASH-S occupies the pocket filled by Cys42-SH in oxidized BACoADR. The nascent Cys42-SH side chain accommodates the CoASH-S shift by adopting a new conformation away from the flavin and interacting with the conserved active-site Tyr367′-OH and Tyr425′-OH at distances of 3.0 and 2.9 Å, respectively. As a result of the slight shift in position of the CoASH-S on reduction and the Cys42-SH conformational change, the two sulfur atoms are separated by 4.0 Å in the NADH and NADPH complexes (Figure 7). While the interaction of Cys42-SH with Tyr367′ and Tyr425′ should stabilize the conjugate thiolate base, this external conformation, which gives a Cys42-SG to FAD-C4a distance of 5.1 Å, is not expected to support the EH_2 charge-transfer absorbance observed in NAD(P)H titrations with BACoADR. While the external conformation observed for Cys42 may well be populated to some extent during catalysis, and while this aspect of the reduced structure gives

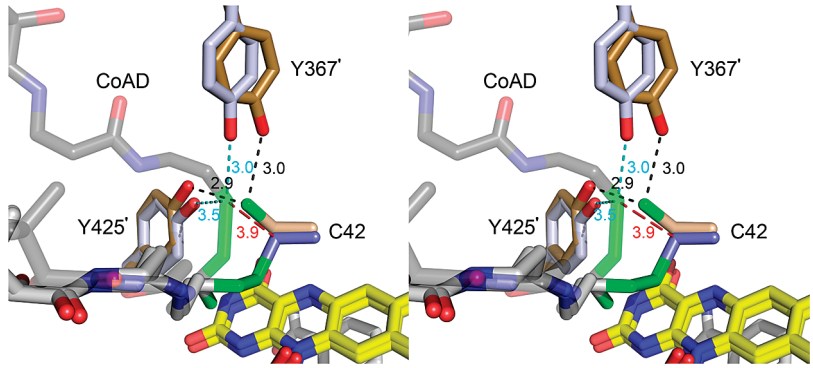

FIGURE 7: Tyr367′ and Tyr425′ interactions with Cys42-SG in the BACoADR-NADH complex and with modeled CoA-disulfide substrate. This view of the oxidized versus NADH-reduced BACoADR overlay (originally described in Figure 6) focuses on the respective FAD centers (with a portion of bound NADH depicted on the distal *re*-face), the reduced and oxidized forms of the Cys42-SSCoA center, and the Tyr residues from chain B. All color-coding is as previously described, with carbon atoms for Cys42 and both Tyr colored as in Figures 4 (oxidized BACoADR) and 5 (BACoADR-NADH). Hydrogen bonds between both Tyr and Cys42-SG in the NADH-reduced structure are given in black dashes. The modeled CoAD substrate (see Figure 7 of ref *12*) was introduced by overlaying the dimeric model of the oxidized SACoADR-CoAS-II complex with oxidized BACoADR. The position of the CoAS-II sulfur is identical to that of the SACoADR chloride ion (*12*). The position of the CoAS-I sulfur (relative to oxidized BACoADR) was adjusted to allow for the proper CoAD disulfide bond length. The distances between the two Tyr-OH (oxidized BACoADR) and the CoAS-II sulfur of modeled CoAD are indicated by cyan dashes, and that between the CoAS-II sulfur and Cys42-CB (oxidized BACoADR) is given with red dashes.

detailed insight into a Cys42-SG position that interacts strongly with the conserved Tyr residues, we conclude that this conformation results from the tightly bound, reduced CoASH (CoAS-I). CoASH dissociation is expected to allow Cys42 to return to the side chain conformation, very similar to that in oxidized BACoADR, which optimizes the EH_2 charge-transfer interaction and promotes the nucleophilic attack on CoAD (see below). Interestingly, a similar "out" conformation for Cys44-SH in the *E. coli* lipoamide dehydrogenase EH_2 form could correspond to the fluorescent species I (see Figure 7 of ref *40*) identified in dithionite titrations.

The environment of Cys42 in the BACoADR-NAD(P)H complex is reminiscent of that for Cys15 in the *B. subtilis* OhrR repressor, as deduced from structural analyses of reduced wild-type OhrR and of the C15S mutant (*52*). Very recently, *S*-thiolation of Cys15, via a Cys15-sulfenic acid intermediate, has been demonstrated *in vivo* with Cys, CoASH, and with a novel 398-Da thiol (*4*). In each case, *S*-thiolation leads to dissociation of the OhrR:operator complex. The apparent pK_a of Cys15-SH is 5.2; the thiolate species is stabilized in part by a positive helix dipole, but there are no basic residues within 7 Å of Cys15-SG. Hydrogen-bonding interactions with Tyr29′-OH and Tyr40′-OH are thought to contribute to the stabilization of Cys15-S^-; a very recent, extensive analysis of Tyr29 and Tyr40 mutants (*53*) demonstrates that both residues are important factors in the peroxide reactivity of Cys15. In addition to their potential effects on Cys15-SH pK_a, Tyr29′ and Tyr40′ may facilitate Cys-sulfenic acid formation either by restricting the orientation of the Cys15 side chain or by protonating the ROH product formed with cumene- and other alkyl hydroperoxides.

Solely on the basis of the refined 1.54 Å structure of oxidized SACoADR, in which Tyr361′-OH interacts strongly with the active-site chloride ion, we proposed (*12*) that this residue might serve a primary role in protonating the nascent CoAS-II thiolate during nucleophilic attack of Cys43-S^- on CoAS-I of the CoAD substrate. Although the external conformation observed for Cys42 in the reduced BACoADR

Scheme 2: Proton Donors and Their Proposed Roles in GR and BACoADR

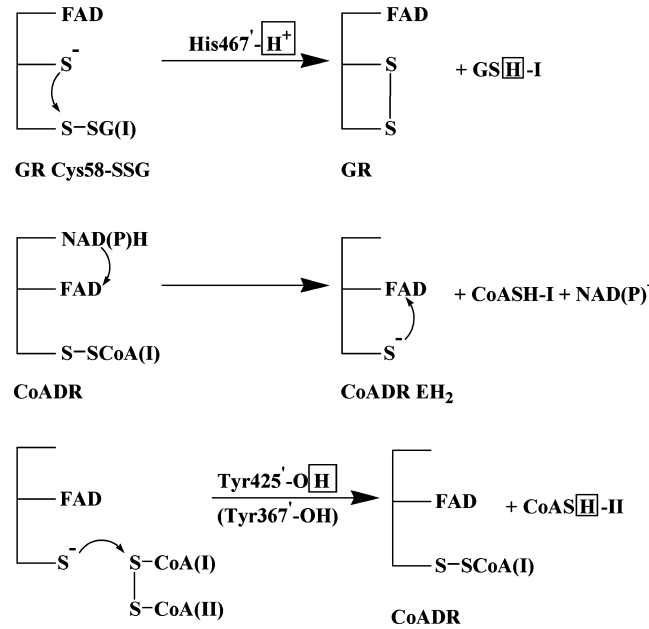

complex does interact strongly with Tyr367′ and Tyr425′, it does not provide an appropriate geometry for nucleophilic attack on CoAS-I; in fact, Cys42-SG of the BACoADR-NADH complex is in contact violation (2.2 Å) with the position of the SACoADR chloride ion (the modeled CoAS-II sulfur of CoAD) in the corresponding overlay. Figure 7 also includes the modeled CoAD substrate as developed with the oxidized SACoADR structure (*12*). As indicated, the CoAS-II sulfur lies 3.9 Å from Cys42-CB and is close to the limiting van der Waals distance for the two atoms. Tyr367′-OH and Tyr425′-OH (oxidized BACoADR) are 3.0 and 3.5 Å, respectively, from the CoAS-II sulfur. There are key similarities (Scheme 2) between the reduction of CoAD by BACoADR (Cys42) and that of GSSG by GR [Cys58 (*8, 44*)]. BACoADR Tyr425 is structurally equivalent to GR His467 [His439 in *E. coli* GR (*54*)]; in the GR(GSSG + $NADP^+$) crystal structure (*44*), the optimal hydrogen-bonding potential for His467′-NE2 lies with the GS-I sulfur. NE2 points most

Table 4: Kinetic Parameters for Wild-Type and Mutant[a] BACoADRs

BACoADR	K_m[NAD(P)H]	K_m(CoAD)	k_{cat}	k_{cat}/K_m[NAD(P)H]
wild-type				
(NADH)	1 μM	2 μM	27 s^{-1}	2.7×10^7 M^{-1} s^{-1}
(NADPH)	3 μM	6 μM	28 s^{-1}	9.3×10^6 M^{-1} s^{-1}
Y367F				
(NADH)			7 s^{-1}	
(NADPH)			5 s^{-1}	
Y425F				
(NADH)			0.9 s^{-1}	
(NADPH)			0.3 s^{-1}	
Y367,425F			0	

[a] Turnover numbers for the mutants were determined in the standard spectrophotometric assay at fixed NAD(P)H and CoAD concentrations.

directly at the GS-I sulfur, at a distance of 3.4 Å, in the GSSG complex; there is no interaction with either Cys58-SG or the GS-II sulfur. As Cys58-SG proceeds to attack GS-I, His467′-NE2 has been proposed to become protonated; this proton is subsequently transferred to the GSH-I product that appears as Cys63-SG reforms the protein disulfide with Cys58. The *E. coli* GR H439A mutant has 0.3% activity, supporting its critical role as an acid−base catalyst in turnover. It should be noted that an alternate interpretation of the GR mutant data (*54*) concludes that His439′ protonates the GS-II sulfur, preventing the facile back-reaction. The GR(GSSG + $NADP^+$) and GR Cys58-SSG(GSH) structures (*44*), however, support the His role in GS-I protonation and product release.

Although certain aspects of the model presented in Figure 7 (e.g., Tyr-OH distances to CoAS-II sulfur in reduced BACoADR, geometry of CoAD disulfide bond relative to Cys42-S) require further analysis, the present work does suggest that Tyr367′ and, in particular, Tyr425′ may be important in BACoADR catalysis. To test this idea, we have evaluated the roles of Tyr367′ and Tyr425′ in BACoADR in standard assays with the corresponding Tyr → Phe mutants and in the Y367,425F double mutant. With NADPH as the reducing substrate, the Y425F mutant is 1% as active as wild-type BACoADR (Table 4), but the Y367F enzyme is more active by an order of magnitude (18% as active as wild-type enzyme). BACoADR Tyr367′ certainly does not perform any essential acid−base function in catalysis. The much lower activity for the Y425F mutant is suggestive of a more critical role for Tyr425′ in catalysis, consistent with its hydrogen-bonding distance (to Cys42-SG) of 2.9 Å. Furthermore, the Y367,425F double mutant has *no* measurable activity in the CoADR assay. Very recently, Tu et al. (*55*) have identified two distinct proton donors in the complex flavoprotein 2,4-dienoyl-CoA reductase, Tyr166 and Glu164. While Tyr166 had earlier been considered essential for the proton transfer step during substrate reduction, the Y166F mutant has 27% activity (similar to that of the BACoADR Y367F mutant). The Y166F/E164Q double mutant, however, has no detectable (<0.01%) activity; in consideration of these results and the crystal structure of an enzyme−product analogue complex, the authors conclude that (1) Tyr166 is not an essential proton donor, (2) Glu164 is a cryptic alternate proton donor, providing this function only in the absence of Tyr166, and (3) His252 interacts with both residues and is an important factor in facilitating their respective proton donor roles. Although Tyr367′-OH and Tyr425′-OH are separated by a distance of 3.8 Å in the BACoADR-NADH complex, each residue interacts with Cys42-SG. Our results, in view of the proton-transfer dyad identified in 2,4-dienoyl-CoA reductase, suggest that Tyr425′ may be the primary proton donor in BACoADR (Scheme 2), protonating the nascent CoAS-II thiolate; in the absence of Tyr425′, this function can be provided by Tyr367′. In this model, the 1% residual activity in the Y425F mutant is thus attributed to Tyr367′ operating as the cryptic alternate donor to the CoAS-II thiolate. The 18% residual activity in the Y367F mutant suggests that it plays a minor role in ensuring the proper environment, perhaps positioning the bound CoAD and/or Tyr425′-OH (Tyr367′-OH···Tyr425′-OH distance = 3.4 Å in oxidized BACoADR). The latter interaction could, for example, reflect a mechanism by which Tyr367′ could facilitate proton transfer from Tyr425′, similar to the role of His252 in 2,4-dienoyl-CoA reductase. In either case, the Y367,425F double mutant lacks any source of the proton required for CoASH-II release and has no detectable CoADR activity.

REFERENCES

1. Leichert, L. I., Scharf, C., and Hecker, M. (2003) Global characterization of disulfide stress in *Bacillus subtilis*. *J. Bacteriol. 185*, 1967–1975.
2. Newton, G. L., Arnold, K., Price, M. S., Sherrill, C., delCardayre, S. B., Aharonowitz, Y., Cohen, G., Davies, J., Fahey, R. C., and Davis, C. (1996) Distribution of thiols in microorganisms: mycothiol is a major thiol in most actinomycetes. *J. Bacteriol. 178*, 1990–1995.
3. Hochgräfe, F., Mostertz, J., Pother, D.-C., Becher, D., Helmann, J. D., and Hecker, M. (2007) *S*-Cysteinylation is a general mechanism for thiol protection of *Bacillus subtilis* proteins after oxidative stress. *J. Biol. Chem. 282*, 25981–25985.
4. Lee, J. W., Soonsanga, S., and Helmann, J. D. (2007) A complex thiolate switch regulates the *Bacillus subtilis* organic peroxide sensor OhrR. *Proc. Natl. Acad. Sci. U.S.A. 104*, 8743–8748.
5. Setlow, B., and Setlow, P. (1977) Levels of acetyl coenzyme A, reduced and oxidized coenzyme A, and coenzyme A in disulfide linkage to protein in dormant and germinated spores and growing and sporulating cells of *Bacillus megaterium*. *J. Bacteriol. 132*, 444–452.
6. Swerdlow, R. D., and Setlow, P. (1983) Purification and characterization of a *Bacillus megaterium* disulfide reductase specific for disulfides containing pantethine 4′,4″-diphosphate. *J. Bacteriol. 153*, 475–484.
7. Ojha, S., Meng, E. C., and Babbitt, P. C. (2007) Evolution of function in the "two dinucleotide binding domains" flavoproteins. *PLoS Comput. Biol. 3*, e121.
8. Argyrou, A., and Blanchard, J. S. (2004) Flavoprotein disulfide reductases: advances in chemistry and function. *Prog. Nucleic Acid Res. Mol. Biol. 78*, 89–142.
9. delCardayre, S. B., Stock, K. P., Newton, G. L., Fahey, R. C., and Davies, J. E. (1998) Coenzyme A disulfide reductase, the primary low molecular weight disulfide reductase from *Staphylococcus aureus*. Purification and characterization of the native enzyme. *J. Biol. Chem. 273*, 5744–5751.
10. delCardayre, S. B., and Davies, J. E. (1998) *Staphylococcus aureus* coenzyme A disulfide reductase, a new subfamily of pyridine nucleotide-disulfide oxidoreductase. Sequence, expression, and analysis of *cdr*. *J. Biol. Chem. 273*, 5752–5757.
11. Luba, J., Charrier, V., and Claiborne, A. (1999) Coenzyme A-disulfide reductase from *Staphylococcus aureus*: evidence for asymmetric behavior on interaction with pyridine nucleotides. *Biochemistry 38*, 2725–2737.
12. Mallett, T. C., Wallen, J. R., Karplus, P. A., Sakai, H., Tsukihara, T., and Claiborne, A. (2006) Structure of coenzyme A-disulfide reductase from *Staphylococcus aureus* at 1.54 Å resolution. *Biochemistry 45*, 11278–11289.
13. Bergman, N. H., Anderson, E. C., Swenson, E. E., Niemeyer, M. M., Miyoshi, A. D., and Hanna, P. C. (2006) Transcriptional profiling of the *Bacillus anthracis* life cycle *in vitro* and an implied model for regulation of spore formation. *J. Bacteriol. 188*, 6092–6100.
14. Liu, H., Bergman, N. H., Thomason, B., Shallom, S., Hazen, A., Crossno, J., Rasko, D. A., Ravel, J., Read, T. D., Peterson, S. N.,

Yates, J., III, and Hanna, P. C. (2004) Formation and composition of the *Bacillus anthracis* endospore. *J. Bacteriol. 186*, 164–178.
15. Antelmann, H., Williams, R. C., Miethke, M., Wipat, A., Albrecht, D., Harwood, C. R., and Hecker, M. (2005) The extracellular and cytoplasmic proteomes of the non-virulent *Bacillus anthracis* strain UM23C1-2. *Proteomics 5*, 3684–3695.
16. Sebaihia, M., Peck, M. W., Minton, N. P., Thomson, N. R., Holden, M. T., Mitchell, W. J., Carter, A. T., Bentley, S. D., Mason, D. R., Crossman, L., Paul, C. J., Ivens, A., Wells-Bennik, M. H., Davis, I. J., Cerdeno-Tarraga, A. M., Churcher, C., Quail, M. A., Chillingworth, T., Feltwell, T., Fraser, A., Goodhead, I., Hance, Z., Jagels, K., Larke, N., Maddison, M., Moule, S., Mungall, K., Norbertczak, H., Rabbinowitsch, E., Sanders, M., Simmonds, M., White, B., Whithead, S., and Parkhill, J. (2007) Genome sequence of a proteolytic (Group I) *Clostridium botulinum* strain Hall A and comparative analysis of the clostridial genomes. *Genome Res. 17*, 1082–1092.
17. Bettegowda, C., Huang, X., Lin, J., Cheong, I., Kohli, M., Szabo, S. A., Zhang, X., Diaz, L. A., Jr., Velculescu, V. E., Parmigiani, G., Kinzler, K. W., Vogelstein, B., and Zhou, S. (2006) The genome and transcriptomes of the anti-tumor agent *Clostridium novyi-NT*. *Nat. Biotechnol. 24*, 1573–1580.
18. Nicely, N. I., Parsonage, D., Paige, C., Newton, G. L., Fahey, R. C., Leonardi, R., Jackowski, S., Mallett, T. C., and Claiborne, A. (2007) Structure of the type III pantothenate kinase from *Bacillus anthracis* at 2.0 Å resolution: implications for coenzyme A-dependent redox biology. *Biochemistry 46*, 3234–3245.
19. Newton, G. L., and Fahey, R. C. (1990) Glutathione in Prokaryotes, in *Glutathione: Metabolism and Physiological Functions* (Vina, J., Ed.), pp 69−77, CRC Press, Boca Raton, FL.
20. Boylan, J. A., Hummel, C. S., Benoit, S., Garcia-Lara, J., Treglown-Downey, J., Crane, E. J., III, and Gherardini, F. C. (2006) *Borrelia burgdorferi* bb0728 encodes a coenzyme A disulfide reductase whose function suggests a role in intracellular redox and oxidative stress response. *Mol. Microbiol. 59*, 475–486.
21. Parsonage, D., Miller, H., Ross, R. P., and Claiborne, A. (1993) Purification and analysis of streptococcal NADH peroxidase expressed in *Escherichia coli*. *J. Biol. Chem. 268*, 3161–3167.
22. Cornish-Bowden, A. (1995) *Fundamentals of Enzyme Kinetics*, Portland Press Ltd., London.
23. Sucharitakul, J., Chaiyen, P., Entsch, B., and Ballou, D. P. (2006) Kinetic mechanisms of the oxygenase from a two-component enzyme, *p*-hydroxyphenylacetate 3-hydroxylase from *Acinetobacter baumannii*. *J. Biol. Chem. 281*, 17044–17053.
24. Yeh, J. I., and Claiborne, A. (2002) Crystal structures of oxidized and reduced forms of NADH peroxidase. *Methods Enzymol. 353*, 44–54.
25. Pflugrath, J. W. (1999) The finer things in X-ray diffraction data collection. *Acta Crystallogr., Sect. D 55*, 1718–1725.
26. Leslie, A. G. W. (1992) Recent changes to the MOSFLM package for processing film and image plate data. Joint CCP4 + ESF-EAMCB Newsletter on Protein Crystallography.
27. Otwinowski, Z., and Minor, W. (1997) Processing of X-ray diffraction data collected in oscillation mode. *Methods Enzymol. 276*, 307–326.
28. Vagin, A., and Teplyakov, A. (1997) MOLREP: an automated program for molecular replacement. *J. Appl. Crystallogr. 30*, 1022–1025.
29. Brunger, A. T., Adams, P. D., Clore, G. M., DeLano, W. L., Gros, P., Grosse-Kunstleve, R. W., Jiang, J. S., Kuszewski, J., Nilges, M., Pannu, N. S., Read, R. J., Rice, L. M., Simonson, T., and Warren, G. L. (1998) Crystallography & NMR system: a new software suite for macromolecular structure determination. *Acta Crystallogr., Sect. D 54*, 905–921.
30. Terwilliger, T. C., and Berendzen, J. (1999) Automated MAD and MIR structure solution. *Acta Crystallogr., Sect. D 55*, 849–861.
31. Terwilliger, T. C. (2000) Maximum-likelihood density modification. *Acta Crystallogr., Sect. D 56*, 965–972.
32. Terwilliger, T. C. (2003) Automated main-chain model building by template matching and iterative fragment extension. *Acta Crystallogr., Sect. D 59*, 38–44.
33. Jones, T. A., Zou, J. Y., Cowan, S. W., and Kjeldgaard, M. (1991) Improved methods for building protein models in electron-density maps and the location of errors in these models. *Acta Crystallogr., Sect. A 47*, 110–119.
34. Abrahams, J. P., and Leslie, A. G. W. (1996) Methods used in the structure determination of bovine mitochondrial F_1 ATPase. *Acta Crystallogr., Sect. D 52*, 30–42.
35. Murshudov, G. N., Vagin, A. A., and Dodson, E. J. (1997) Refinement of macromolecular structures by the maximum-likelihood method. *Acta Crystallogr., Sect. D 53*, 240–255.
36. Emsley, P., and Cowtan, K. (2004) Coot: model-building tools for molecular graphics. *Acta Crystallogr., Sect. D 60*, 2126–2132.
37. Winn, M. D., Isupov, M. N., and Murshudov, G. N. (2001) Use of TLS parameters to model anisotropic displacements in macromolecular refinement. *Acta Crystallogr., Sect. D 57*, 122–133.
38. Williams, C. H., Jr. (1976) Flavin-Containing Dehydrogenases, in *The Enzymes* (Boyer, P. D., Ed.) Vol. XIII, 3rd ed., pp 89−173, Academic Press, New York.
39. Williams, C. H., Jr. (1992) Lipoamide Dehydrogenase, Glutathione Reductase, Thioredoxin Reductase, and Mercuric Ion Reductase - A Family of Flavoenzyme Transhydrogenases, in *Chemistry and Biochemistry of Flavoenzymes* (Muller, F., Ed.), Vol. III, pp 121−211, CRC Press, Boca Raton, FL.
40. Wilkinson, K. D., and Williams, C. H., Jr. (1979) Evidence for multiple electronic forms of two-electron-reduced lipoamide dehydrogenase from *Escherichia coli*. *J. Biol. Chem. 254*, 852–862.
41. Hopkins, N., and Williams, C. H., Jr. (1995) Characterization of lipoamide dehydrogenase from *Escherichia coli* lacking the redox active disulfide: C44S and C49S. *Biochemistry 34*, 11757–11765.
42. Hopkins, N., and Williams, C. H., Jr. (1995) Lipoamide dehydrogenase from *Escherichia coli* lacking the redox active disulfide: C44S and C49S. Redox properties of the FAD and interactions with pyridine nucleotides. *Biochemistry 34*, 11766–11776.
43. Dym, O., and Eisenberg, D. (2001) Sequence-structure analysis of FAD-containing proteins. *Protein Sci. 10*, 1712–1728.
44. Karplus, P. A., and Schulz, G. E. (1989) Substrate binding and catalysis by glutathione reductase as derived from refined enzyme: substrate crystal structures at 2 Å resolution. *J. Mol. Biol. 210*, 163–180.
45. Lountos, G. T., Jiang, R., Wellborn, W. B., Thaler, T. L., Bommarius, A. S., and Orville, A. M. (2006) The crystal structure of NAD(P)H oxidase from *Lactobacillus sanfranciscensis*: insights into the conversion of O_2 into two water molecules by the flavoenzyme. *Biochemistry 45*, 9648–9659.
46. Stehle, T., Claiborne, A., and Schulz, G. E. (1993) NADH binding site and catalysis of NADH peroxidase. *Eur. J. Biochem. 211*, 221–226.
47. Scrutton, N. S., Berry, A., and Perham, R. N. (1990) Redesign of the coenzyme specificity of a dehydrogenase by protein engineering. *Nature 343*, 38–43.
48. van Petegem, F., de Vos, D., Savvides, S., Vergauwen, B., and van Beeumen, J. (2007) Understanding nicotinamide dinucleotide cofactor and substrate specificity in class I flavoprotein disulfide oxidoreductases: crystallographic analysis of a glutathione amide reductase. *J. Mol. Biol. 374*, 883–889.
49. Vergauwen, B., Pauwels, F., Jacquemotte, F., Meyer, T. E., Cusanovich, M. A., Bartsch, R. G., and van Beeumen, J. J. (2001) Characterization of glutathione amide reductase from *Chromatium gracile*. Identification of a novel thiol peroxidase (Prx/Grx) fueled by glutathione amide redox cycling. *J. Biol. Chem. 276*, 20890–20897.
50. Holm, L., and Park, J. (2000) DaliLite workbench for protein structure comparison. *Bioinformatics 16*, 566–567.
51. Krauth-Siegel, R. L., Arscott, L. D., Schonleben-Janas, A., Schirmer, R. H., and Williams, C. H., Jr. (1998) Role of active site tyrosine residues in catalysis by human glutathione reductase. *Biochemistry 37*, 13968–13977.
52. Hong, M., Fuangthong, M., Helmann, J. D., and Brennan, R. G. (2005) Structure of an OhrR-*ohrA* operator complex reveals the DNA binding mechanism of the MarR family. *Mol. Cell 20*, 131–141.
53. Soonsanga, S., Fuangthong, M., and Helmann, J. D. (2007) Mutational analysis of active site residues essential for sensing of organic hydroperoxides by *Bacillus subtilis* OhrR. *J. Bacteriol. 189*, 7069–7076.
54. Rietveld, P., Arscott, L. D., Berry, A., Scrutton, N. S., Deonarain, M. P., Perham, R. N., and Williams, C. H., Jr. (1994) Reductive and oxidative half-reactions of glutathione reductase from *Escherichia coli*. *Biochemistry 33*, 13888–13895.
55. Tu, X., Hubbard, P. A., Kim, J. J., and Schulz, H. (2008) Two distinct proton donors at the active site of *Escherichia coli* 2,4-dienoyl-CoA reductase are responsible for the formation of different products. *Biochemistry 47*, 1167–1175.

BI8002204